JGR Space Physics

RESEARCH ARTICLE
10.1029/2019JA026815

A New Perspective for Dipolarization Front Dynamics: Electromagnetic Effects of Velocity Inhomogeneity

Dong Lin[1], Wayne A. Scales[1], Gurudas Ganguli[2], Xiangrong Fu[3], Chris Crabtree[2], Erik Tejero[2], Yuxi Chen[4], and Alex C. Fletcher[2]

[1]Bradley Department of Electrical and Computer Engineering, Virginia Polytechnic Institute and State University, Blacksburg, VA, USA, [2]Naval Research Lab, Washington, DC, USA, [3]New Mexico Consortium, Los Alamos, NM, USA, [4]Center for Space Environment Modeling, University of Michigan, Ann Arbor, MI, USA

Key Points:
- Magnetotail DF contains a substantial velocity shear in the tangential electron drift
- The sheared flow is susceptible to the EIH instability and can broaden the DF by emitting broadband LH waves
- The EIH emissions become more electromagnetic as plasma beta increases

Correspondence to:
D. Lin,
ldong7@vt.edu

Citation:
Lin, D., Scales, W. A., Ganguli, G., Fu, X., Crabtree, C., Tejero, E. M., et al. (2019). A new perspective for dipolarization front dynamics: Electromagnetic effects of velocity inhomogeneity. *Journal of Geophysical Research: Space Physics*, *124*, 7533–7542. https://doi.org/10.1029/2019JA026815

Received 9 APR 2019
Accepted 4 AUG 2019
Accepted article online 7 SEP 2019
Published online 12 SEP 2019

Abstract The stability of a quasi-static near-Earth dipolarization front (DF) is investigated with a two-dimensional electromagnetic particle-in-cell model. Strongly localized ambipolar electric fields self-consistently generate a highly sheared dawnward $\vec{E} \times \vec{B}$ electron drift on the kinetic scale in the DF. Electromagnetic particle-in-cell simulations based on the observed DF thickness and gradients of plasma/magnetic field parameters reveal that the DF is susceptible to the kinetic electron-ion hybrid (EIH) instability driven by the strong velocity inhomogeneity. The excited waves show a broadband spectrum in the lower hybrid (LH) frequency range, which has been often observed at DFs. The wavelength is comparable to the shear scale length, and the growth rate is also in the LH frequency range, which are consistent with the EIH theory. As a result of the LH wave emissions, the velocity shear is relaxed, and the DF is broadened. When the plasma beta increases, the wave mode shifts to longer wavelengths with reduced growth rates and enhanced magnetic fluctuations although the wave power is mostly in the electrostatic regime. This study highlights the role of velocity inhomogeneity in the dynamics of DF which has been long neglected. The EIH instability is suggested to be an important mechanism for the wave emissions and steady-state structure at the DF.

1. Introduction

Dipolarization fronts (DFs) are earthward propagating boundary layer structures that are frequently observed in the Earth's magnetotail. The most prominent feature of DFs is a sharp increase of magnetic field northward component over a scale length comparable to or less than the ion thermal gyroradius (Runov et al., 2009, 2011). DFs are generally believed to be generated by magnetotail reconnection. When the hot and tenuous reconnection jet encounters the denser and colder ambient magnetotail plasma, the kinetic-scale boundary layer is formed (e.g., Lu et al., 2015; Sitnov et al., 2009). The inhomogeneities of plasma and magnetic field parameters at DFs are expected to excite a number of wave modes. Waves with a broad frequency range are observed to coincide with the DF, with frequencies extending from below the lower hybrid (LH) frequency to above the electron cyclotron frequency (e.g., Zhou et al., 2009).

The strong earthward density gradient at DFs has been shown to drive a hierarchy of instabilities on different scales. Runov et al. (2011) revealed that the plasma density typically decreases by ~50% at the tailward side of DF. Lapenta and Bettarini (2011) found with 3-D magnetohydrodynamic simulations that the density gradient at the DFs can lead to an interchange instability, the scale of which is selected by the kinking flux ropes upstream. Pritchett and Coroniti (2010) found with 3-D electromagnetic particle-in-cell (EMPIC) simulations that the dipolarized plasma sheet configuration is unstable to a ballooning-/interchange-type mode, which has a wavelength on the order of the ion gyroradius. This mode can be interpreted as the low-frequency extension of the LH drift instability (LHDI). The evolution of LHDI at DF has also been investigated by Divin, Khotyaintsev, Vaivads, André, Markidis, and Lapenta (2015) and Divin, Khotyaintsev, Vaivads, and André (2015). It was found that the density gradient-driven LHDI generates wave modes on the electron gyroradius scale with frequencies in the LH range (Krall & Liewer, 2014).

The anisotropic velocity distributions are another energy source of unstable modes at the magnetotail DFs. Fu, Khotyaintsev, Vaivads, André, Sergeev, et al. (2012) examined the pitch angle distribution of suprathermal electrons in the flux pileup regions located behind the DFs. They found perpendicular ($T_{\perp,e}/T_{\parallel,e} > 1$)

and parallel ($T_{\perp,e}/T_{\parallel,e} < 1$) distributions inside the growing and decaying flux pileup regions, respectively. These distributions are suggested to result from betatron acceleration due to the magnetic field compression and Fermi acceleration due to the shrinkage of a flux tube (Fu et al., 2011; Huang et al., 2015; Lu, Angelopoulos, & Fu, 2016) and could drive the temperature anisotropy whistler instability and oblique electron firehose instability, respectively (Zhang et al., 2018).

While the density gradient- and anisotropy-driven instabilities have been investigated in a number of studies, the effects of flow inhomogeneity within the DF has been long neglected. The strong gradient of magnetic field B_Z at DFs implies the existence of a current density in the dusk direction, which has been verified by satellite observations (e.g., Fu, Khotyaintsev, Vaivads, André, & Huang, 2012). The current density was shown to be mainly carried by the dawnward drifting electron flow, which consists of both diamagnetic drift due to electron pressure gradient and the $\vec{E} \times \vec{B}$ drift due to the earthward electric field. Note here the ions are effectively unmagnetized in the DF thus cannot undergo the drift motion entirely (Ganguli et al., 2018; Wu & Shay, 2012). The transverse electric field is essentially an earthward ambipolar electric field due to the global compression effects and localized in the DF. Further quantitative analysis reveal that the $\vec{E} \times \vec{B}$ drift is dominant over the diamagnetic drift and ion flow is relatively negligible (Fletcher et al., 2019; Fu, Khotyaintsev, Vaivads, André, & Huang, 2012). Considering the kinetic-scale thickness, the electron flows within the DFs are shown to have a substantial velocity shear, the electromagnetic effects of which on the DF stability, however, have not been well explored before (Fletcher et al., 2019; Ganguli et al., 2018).

Velocity shear-driven instabilities are ubiquitous in space plasma environments on different scales. Depending on the shear scale length L_E relative to the ion gyroradius ρ_i, the consequent wave modes have different wave frequencies and wavelengths that are commensurate with the velocity shear (Ganguli, Keskinen, et al., 1994; Ganguli, Romero, et al., 1994). The classical Kelvin-Helmholtz instability is in the fluid regime $L_E \gg \rho_i$, which can be observed on, for example, the Earth's magnetopause (Hasegawa et al., 2004). The wave frequency is much less than the ion gyrofrequency Ω_{ci}, and the wavelength is much longer than ρ_i (Lin et al., 2014). Kinetic theories have been developed to characterize the unstable wave modes when L_E is comparable to or smaller than ρ_i. Specifically, the electron-ion hybrid (EIH) instability is driven by the transverse velocity shear with intermediate scale length ($\rho_e < L_E < \rho_i$), when ions are effectively unmagnetized and electrons have shear corrected velocity distributions (e.g., Ganguli et al., 1988a, 1988b; Romero et al., 1992). The kinetic EIH modes have been verified in a number of space and laboratory experiments and numerical simulations (e.g., Amatucci et al., 1996; DuBois et al., 2014; Liu et al., 2014, 2017; Romero & Ganguli, 1993; Scales, Bernhardt, & Ganguli, 1994; Scales, Bernhardt, Ganguli, Siefring, & Rodriguez, 1994) and are suggested to be important mechanisms for the generation of broadband electrostatic fluctuations. However, previous EIH studies have been mostly focused on the electrostatic emissions and assumed uniform magnetic field for simplicity (e.g., Romero & Ganguli, 1993; Romero et al., 1992). EIH modes in a more realistic configuration of a DF with magnetic gradient and their nonlinear electromagnetic properties have not been well understood.

Recently, Ganguli et al. (2018) showed with high-resolution Magnetospheric Multiscale (MMS) measurements that the ambipolar potential across the DF results in strongly sheared electron flows with sub-ion scale. Liu et al. (2018) reported MMS observation of an electron jet inside a DF that has a shear frequency larger than the LH frequency. Fletcher et al. (2019) investigated two DF events observed by the MMS satellite and developed a rigorous kinetic equilibrium. It still remains unclear how the highly sheared tangential flow may contribute to the distinctive broadband emissions at DFs. In this study, we evaluate the role of the velocity shear at DFs by investigating the excitation of the electromagnetic EIH instability (Ganguli et al., 2014) at a kinetic-scale boundary layer with sharp gradients of magnetic and plasma parameters. EMPIC simulations are conducted to explore the DF stability and consequent spectral characteristics.

2. Model Configuration

Figure 1 shows the configuration of transverse sheared flows in a magnetotail DF structure. The magnetic field at the DF is characterized by enhanced northward component B_Z with a tailward gradient. An earthward ambipolar electric field E_X is localized within the front due to the compression of magnetotail reconnection outflow, which drives $\vec{E} \times \vec{B}$ drift flow toward the dawn. The gradient scale length of the DF is chosen to be intermediate between the ion and electron gyroradius so that ions are effectively unmagnetized within the DF while electrons are magnetized. The dawnward $\vec{E} \times \vec{B}$ drift and diamagnetic drift of electrons

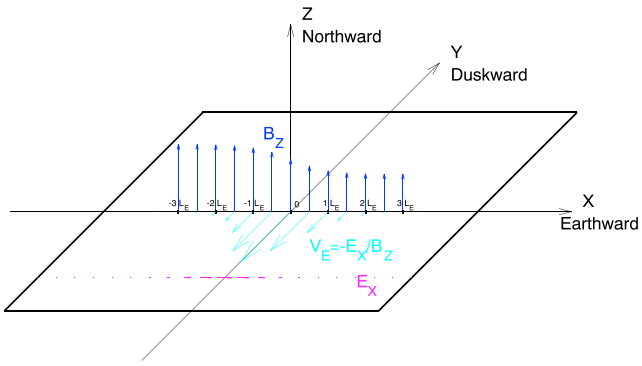

Figure 1. Transverse-sheared electron flow in the equatorial plane of a dipolarization front. The blue arrows show the northward magnetic field B_Z with a tailward gradient. The magenta arrows show the earthward ambipolar electric field. The cyan arrows show the dawnward drift velocity of electron.

result in a net current density toward the duskside. Although we choose a DF in the equatorial plane, our approach is valid to off equatorial DFs as long as the criterion that the scale size normal to the DF (of the order of an ion gyroradius) is much smaller than in the other orthogonal directions (of the order of several Earth radii). As explained in Ganguli et al. (2018), under this condition, the physics in the normal direction is only weakly coupled to the other orthogonal directions and the problem essentially reduces to 1-D as far as the kinetic and fast processes, such as wave generation in and around the LH frequency, are concerned. The model we used for simulation is consistent with the fully kinetic treatment but easier to implement. However, for slow magnetohydrodynamic-scale processes, other dimensions are important as well.

In this study, we adopt a force-balanced model by assuming the ambipolar electric field is localized in the DF and the density profile has a smooth transition of hyperbolic tangent form. The force balance is achieved between the pressure gradient force, $\vec{J}\times\vec{B}$ force, and the electric force. The B_Z profile can be then determined from Ampere's Law. This is a simplified representation of the fully kinetic model in the strong shear region. As explained in Ganguli et al. (2018) and Fletcher et al. (2019), there are stronger gradients on the order of a few electron gyroradius within the DF. These are the likely regions where the waves will first emerge, and hence, we simulate this region. Within this region, $\rho_e \ll L_E \ll \rho_i$, and the electric field may be modeled by equation (1) and the density gradient by equation (2). Equation (3) is the Maxwell equation which leads to the magnetic field pileup as shown in equation (4).

$$E_X(x) = E_m \mathrm{sech}^2 \frac{x}{L_E}, \tag{1}$$

$$N(x) = N_0[1 + \frac{\Delta N}{2}(\tanh \frac{x}{L_E} - 1)], \tag{2}$$

$$\nabla \times \vec{B} = \mu_0 N_e q_e (\vec{V}_{\mathrm{dim}} + \vec{V}_{\vec{E}\times\vec{B}}), \tag{3}$$

$$B_Z(x) = B_0 \sqrt{1 + \beta_0(1 - \frac{N(x)}{N_0}) + \frac{N_0}{\Delta N}\frac{eE_m L_E}{B_0^2/2\mu_0}[1 - (\frac{N(x)}{N_0})^2]}. \tag{4}$$

Here E_X is the earthward ambipolar electric field. $N(x)$ is the distribution of ion number density along the X direction. $\vec{B}$ is the northward magnetic field along the Z direction. $B_Z(x)$ is the magnetic field distribution along the X direction derived from Ampere's Law. L_E is the shear scale length. E_m is the peak value of the electric field. N_0, B_0, and β_0 are the number density, magnetic field, and electron plasma β earthward of DF, respectively. ΔN is the ratio of density drop from Earthward to tailward relative to N_0. N_e is the electron number density, which is approximately equal to the ion number density and satisfies Gauss' Law. μ_0 is the magnetic permeability in vacuum. q_e is the electric charge of an electron. $\vec{V}_{\mathrm{dim}}$ is the diamagnetic drift velocity of electrons: $\frac{-\nabla P_e \times \vec{B}}{N_e q_e B^2}$. $\vec{V}_{\vec{E}\times\vec{B}}$ is the $\vec{E}\times\vec{B}$ drift velocity of electrons: $\frac{\vec{E}\times\vec{B}}{B^2}$. The two drifts represent the

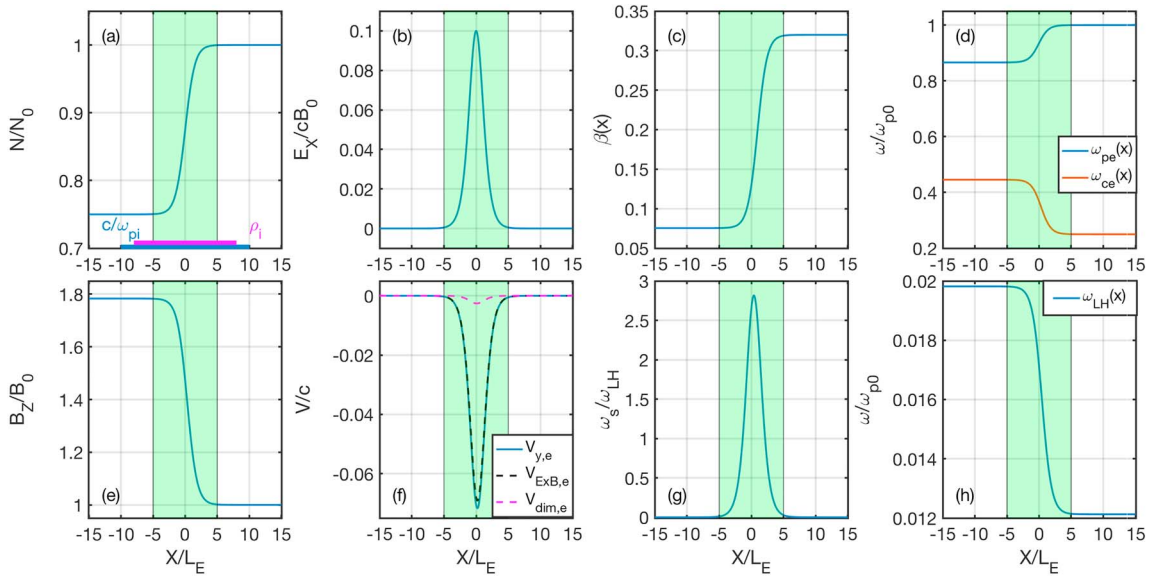

Figure 2. Initial profiles of (a) plasma density; (b) electric field E_X; (c) plasma β; (d) electron plasma frequency ω_{pe} (blue) and electron cyclotron frequency ω_{ce} (orange); (e) magnetic field B_Z; (f) electron total drift velocity (blue), $\vec{E}\times\vec{B}$ drift (black dash), and diamagnetic drift (magenta); (g) ratio between shear frequency ω_s and the lower hybrid frequency ω_{LH}; and (h) lower hybrid frequency ω_{LH}. The green shaded regions show the dipolarization front thickness represented by the transitions of electromagnetic/plasma parameters.

electron responses to different driving forces, which affect the wave generation differently especially when the gradient scale size becomes of the order of an ion gyroradius or less (Fletcher et al., 2019).

Figure 2 shows the initial profiles of the plasma parameters and electromagnetic field components in the DF model. The X axis is pointing toward the Earth. The values are derived from the observed event in Ganguli et al. (2018) but have been adapted to accommodate the simulation capacity. Figures 2a and 2e show the plasma density and magnetic field B_Z, which both use the values on the earthward side as units. The plasma density has an earthward gradient and drops by 25% tailward of the DF. B_Z increases to about 1.8 B_0 in the tailward direction as a result of force balance. Note in the observation, the tailward B_Z is about 1.9 B_0 (from ~7 to ~13 nT). This can be seen as the magnetic field generated by the $\vec{E}\times\vec{B}$ drifting electrons with nearly stationary ions because of negligible gyroaveraged ion $\vec{E}\times\vec{B}$ drift due to the small-scale electric field. Figures 2b and 2f show the ambipolar electric field E_X and the electron dawnward drift velocities. The E_X has an peak value of $E_m = 0.1cB_0$. Here c is the light speed. The electron velocity is dominated by the $\vec{E}\times\vec{B}$ drift, with peak magnitude $0.069c$. The peak magnitude of the diamagnetic drift is $0.003c$. Figure 2c shows the electron plasma $\beta_e = \frac{NkT_0}{B_Z^2/2\mu_0}$ varies from 0.08 in the tailward to 0.32 in the earthward regions. Note $\beta_e = 0.6$ in the observation of Ganguli et al. (2018). Here the ion and electron temperatures are assumed to be uniform for simplicity , that is, neither ion nor electron temperatures have spatial gradient. Figure 2g shows the ratio between the shear frequency ω_s and the LH frequency ω_{LH}. The shear frequency is defined as $\omega_s = V_{y,e}/L_E$ and describes the inhomogeneity of the electron flow. Here the ratio ω_s/ω_{LH} is up to 3 within the unstable range. The electron plasma frequency $\omega_{pe} = \sqrt{\frac{Ne^2}{\epsilon_0 m_e}}$ and electron cyclotron frequency $\omega_{ce} = \frac{eB_Z}{m_e}$ are shown in Figure 2d in blue and orange, respectively. The LH frequency $\omega_{LH} = \frac{\omega_{pi}}{\sqrt{1+(\frac{\omega_{pe}}{\omega_{ce}})^2}}$ is shown in Figure 2h. The three frequencies are shown in unit of the electron plasma frequency $\omega_{p0} = \sqrt{\frac{N_0 e^2}{\epsilon_0 m_e}}$ earthward of the DF.

In this study, we use an electron thermal speed of $V_{the} = 0.1c$ and ion/electron temperature ratio of 4: $T_e = T_i/4 = T_0$. The ratio between electron plasma frequency and gyrofrequency on the earthward side is $\omega_{pe}/\omega_{ce} = 4$. A reduced mass ratio between ion and electron is assumed $m_i/m_e = 400$. The ion and electron gyroradius on the Earthward side are $\rho_i = 16c/\omega_{pe}$ and $\rho_e = 0.4c/\omega_{pe}$, respectively. Here we choose the initial value of $L_E = 1.5c/\omega_{pe} = \rho_i/10.67 = 3.75\rho_e$ in the simulation so that ions can be effectively unmagnetized and electrons magnetized. The green shaded boxes in Figure 2 show the transition regions of the electromagnetic and plasma parameter profiles, which provide a rough estimation of the DF thickness

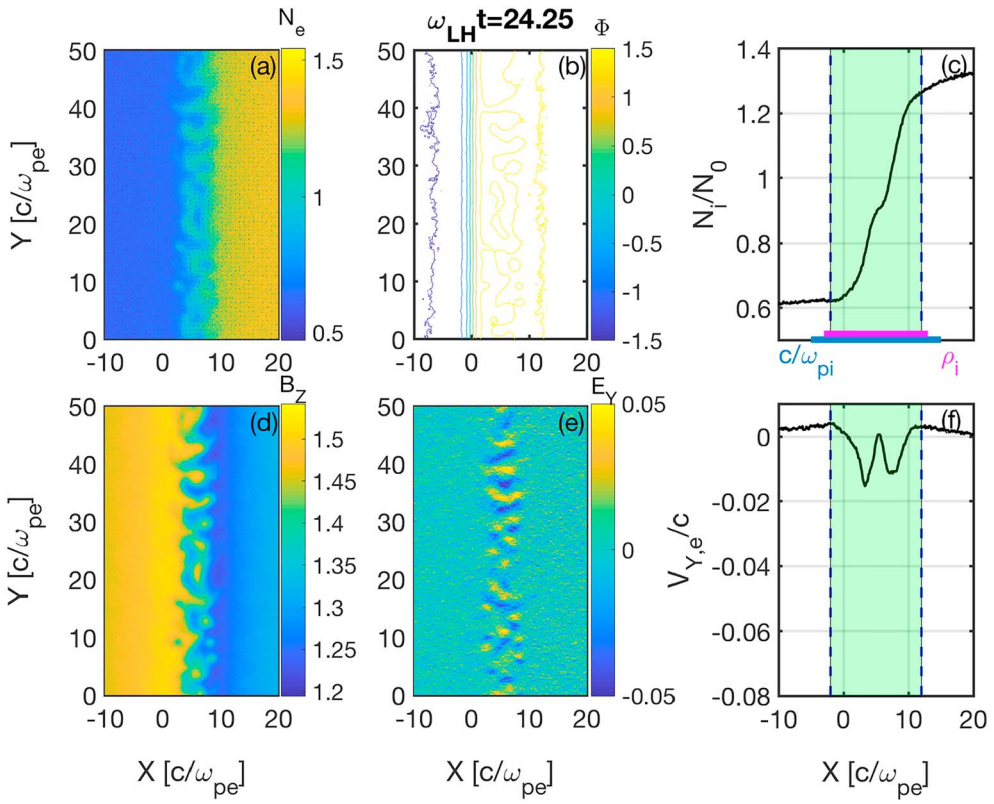

Figure 3. Plasma and electromagnetic field variables at $t = 24.25\ \omega_{\mathrm{LH0}}^{-1}$: (a) electron number density N_e, (b) electrostatic potential Φ, (c) cross section of ion density N_i, (d) B_Z, (e) E_Y, and (f) cross section of electron flow $V_{y,e}$.

as was used in observational analysis (e.g., Runov et al., 2011; Schmid et al., 2014). Note that the initial DF thickness is ~10 c/ω_{pe}, considering the hyperbolic function form, and that the observed DF thickness is related to the saturated status of the instability. The DF thickness in this simulation is basically comparable to the ion scale length and consistent with observations (e.g., Fu, Khotyaintsev, Vaivads, André, & Huang, 2012; Ganguli et al., 2018; Liu et al., 2018). The Alfvén speed based on B_0 and N_0 is $V_{A0} = 0.25c$.

The EMPIC model we used is two-dimensional in the configuration space with three velocity components (2D3V). Both ions and electrons are fully kinetic, and the full set of Maxwell's equations are solved. In order to make use of the periodic boundary conditions, the simulation domain is doubled in the X direction and made symmetric about $x = L_X/2$. The system length is $L_X = 100c/\omega_{pe}$ and $L_Y = 50c/\omega_{pe}$ with $N_X \times N_Y = 1,024 \times 512$ grid cells. The mean number of macroparticles per cell per species is 200. The time step is $0.01\omega_{p0}^{-1}$. Since the LH time scale is the natural time scale in the system, we use $\omega_{\mathrm{LH0}}^{-1}$ as the unit where ω_{LH0} is the LH frequency earthward of the DF.

3. Simulation Results

3.1. EIH Wave Spectrum

Figure 3 shows the plasma density, electron velocity, and electromagnetic fields at $t = 24.25\ \omega_{\mathrm{LH0}}^{-1}$ when the instability has evolved into the nonlinear stage. Figure 3a shows rolled-up vortex structuring in the electron number density (N_e), which is characteristic of the EIH instability (Romero & Ganguli, 1993). Figures 3b, 3d, and 3e show coherent structures in the electrostatic potential Φ, B_Z, and E_Y. A rough estimation of the dominant wavelength is $4.2c/\omega_{pe}$, which is comparable to the shear scale length. Figures 3c and 3f show that the ion number density (N_i) still maintains a strong gradient while the electron sheared flow ($V_{y,e}$) has been mostly depleted. The saturated DF layer is broadened to ~14 $c/\omega_{pe} = 0.7\ c/\omega_{pi} = 0.9\ \rho_i$, which is consistent with observations. Note the flow channel has a displacement along X due to the net magnetic gradient force as the ambipolar electric field is depleted by the instability.

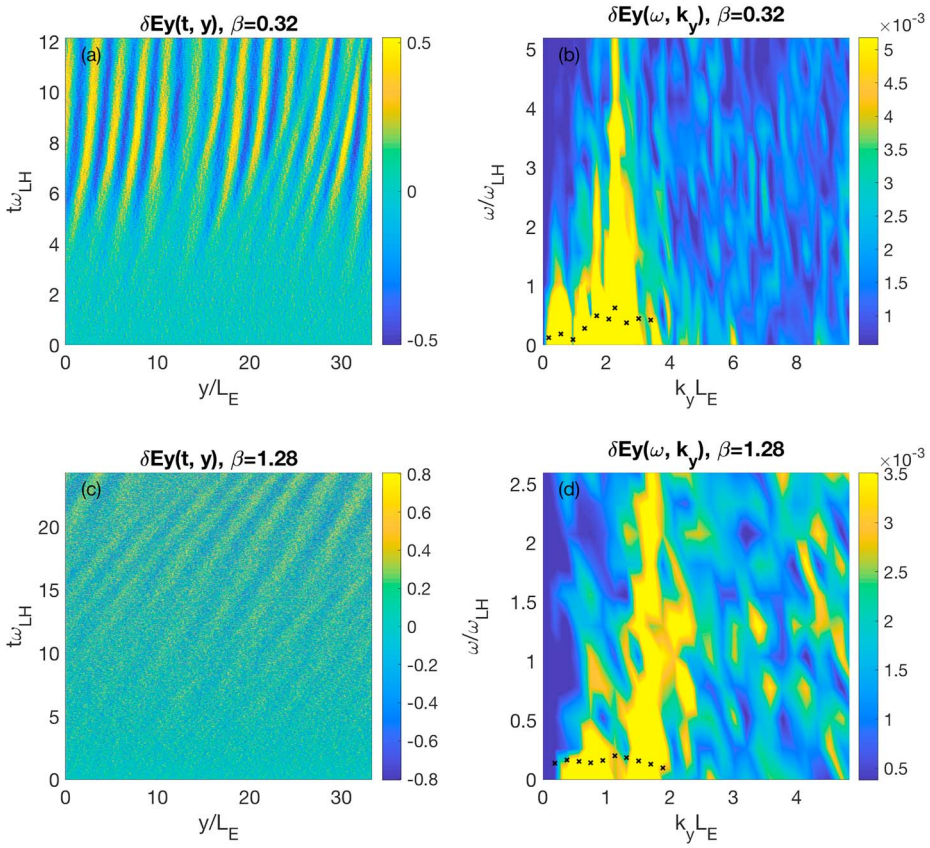

Figure 4. Wave mode characterization. (a,b) Time history of E_Y perturbation sampled along the flow direction in the dipolarization front and the dispersion relation of the sampled E_Y. The black crosses indicate the growth rates of each k_y mode. (c,d) Sampled E_Y perturbation time history and its dispersion relation for another test of $\beta = 1.28$ in the same format with (a) and (b).

In order to further characterize the wave modes, we sample the transverse electric field perturbation of E_Y along the flow channel in the DF. The time history of the one-dimensional sampling is shown in Figure 4a. It can be seen that periodic wave structures start to show up at $\sim 3\omega_{\mathrm{LH}}^{-1}$. The wave fronts represented by the alternating strips indicate that the wave mode is propagating along the Y positive axis toward the dusk. The phase velocity estimated from the slope of the wave front is $\sim 0.004c$, which is comparable to the ion thermal velocity.

A two-dimensional Fourier analysis is applied to the space-time sampling of electric field perturbations shown in Figure 4a. The consequent dispersion relation is shown in Figure 4b. It can be seen that the dominant wave number is around $k_y L_E = 2$ and the frequency is broadband from 0 to $5\omega_{\mathrm{LH}}$. At each sampled time, a spatial Fourier analysis is conducted to get the spectrum power of different wave numbers. The time history of the spectrum power for one k_y mode is linearly fitted to estimate the growth rate of that mode. The growth rates of a few wave modes around the dominant mode are indicated by the black crosses shown in Figure 4b. It can be seen that the fastest growth rate is also on the order of the LH frequency. The dispersion relation shown in Figures 4a and 4b is consistent with the EIH theory that the fastest growing mode has a wavelength comparable to the shear scale length, the real frequency is broadband in the LH range, and the fastest growing mode has a growth rate comparable to the LH frequency (Romero et al., 1992).

3.2. EIH Dependence on Plasma β

We also explored the wave properties dependence on the plasma β. Another simulation was conducted in which the plasma thermal velocity is increased by a factor of 2 so that the plasma β in the earthward direction is 1.28. The density gradient, driving electric field, and shear scale length are kept the same. The maximum B_Z at the tailward direction is slightly increased from $1.78B_0$ to $1.85B_0$. The wave structure and dispersion properties in the DF are shown in Figures 4c and 4d in the same format with Figures 4a and 4b. The wave

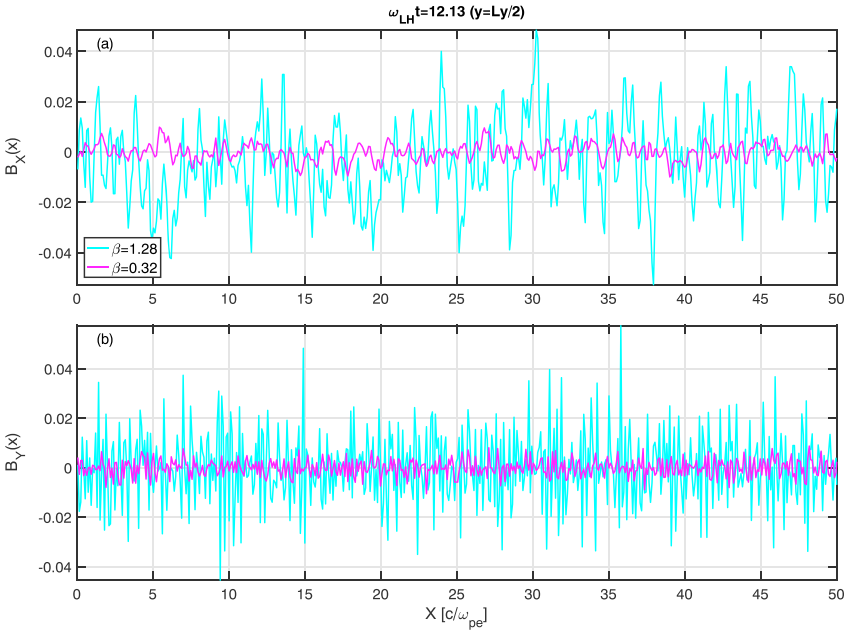

Figure 5. Comparison of electromagnetic perturbations between low and high β. The magnetic field components (a) B_X and (b) B_Y sampled along the X direction at $Y = L_Y/2$ are shown for two runs: $\beta = 0.32$ (magenta) and $\beta = 1.28$ (cyan).

pattern becomes visible after ~10 $\omega_{\mathrm{LH}}^{-1}$ (Figure 4c). The dispersion relation in Figure 4d indicates that the LH spectrum shrinks to a lower frequency band. The fastest growing wave number shifts to smaller values around $k_y L_E \sim 1$. The growth rate is reduced as the plasma β is higher. This is consistent with the theory (Ganguli et al., 2014) and observations of DF which indicate that the wave power is concentrated in the electrostatic regime.

The effects of plasma β are further evaluated by plotting the electromagnetic perturbations from the two simulations with low and high plasma β. Figure 5 shows the B_X and B_Y sampled at $t = 12.13\omega_{\mathrm{LH}}^{-1}$ and $y = L_Y/2$ along the X direction. The results from the high β simulation are shown in cyan and from the low β in magenta. The magnetic perturbations in the high β simulation has a much larger amplitude than those from the low β simulation. Considering that the background magnetic field is only different by 4% and that the high β case has much lower growth rate, the direct comparison of magnetic perturbations here imply that the fluctuations driven by the transverse velocity shear at the DF are more electromagnetic with a higher β.

4. Discussion and Conclusion

In this study, we investigated the velocity shear effects in the magnetotail DF with a two-dimensional EMPIC model. A simplified configuration is adopted in which the DF is treated as a boundary layer with an earthward plasma density gradient, a tailward magnetic field B_Z gradient, and an earthward ambipolar electric field E_X. The velocity shear mainly results from the inhomogeneous electric field that represents the global compression effects. The particle distribution is deviated from Maxwellian, which provides the free energy for the EIH wave emission.

It should be pointed out that the EIH mechanism is different from the LHDI. First, the energy source of EIH instability is the velocity shear, while the LHDI is driven by density gradient. The EIH does not require a density gradient (Figure 3c) but depletes the velocity shear and relaxes the DF (Figure 3f; Romero et al., 1992). This may explain why DF electron jets are not commonly reported although a statistical survey is needed to evaluate the occurrence. Second, the saturated EIH state is featured by vortex structure (Figure 3a), distinct from the "finger" structures of LHDI (Divin, Khotyaintsev, Vaivads, André, Markidis, & Lapenta, 2015; Pritchett & Coroniti, 2010). On the other hand, uniform $\vec{E}\times\vec{B}$ drift velocity is typically assumed for the study of the LHDI (e.g., Daughton, 2003). This may be problematic for DF studies since when the scale size

of the density gradient becomes comparable to an ion gyroradius (as typically found in DFs), the assumption of uniform drift does not hold (Ganguli et al., 2018).

The DF thickness in the simulations presented in this study is representative of the ion scale length as has been found in observations (e.g., Fu, Khotyaintsev, Vaivads, André, & Huang, 2012; Ganguli et al., 2018; Liu et al., 2018; Runov et al., 2009, 2011; Schmid et al., 2014). Note that the DF thickness in observations are usually estimated with the timing method. This method derives the propagation velocity of the DF based on two or more satellites that are close enough to each other and estimates the duration of DF passing with the local minimum and maximum of the magnetic field profile. The DF thickness is then estimated as the product of the propagation velocity and duration time. In this simulation study, the model is set in the frame of the DF; thus, there are no propagation effects. The magnetic profile is simplified with a hyperbolic tangent like function; thus, there are no local maximum or minimum. Instead, the DF thickness is estimated with the distance between the asymptotic points of the profile. It should be clarified that the shear scale length L_E used in this initialization is 1.5 c/ω_{pe}, which is equivalent to 0.075 c/ω_{pi}. However, the DF thickness based on the method typically used in observations is about 10 c/ω_{pe}, as shown by the green shaded boxes in Figure 2. This thickness is equivalent to 0.5 c/ω_{pi} or 0.6 ρ_i, as shown by the blue and magenta bars in Figure 2, respectively. The DF thickness is broadened as a result of the wave emission driven by the EIH instability. As shown in Figure 3c, the DF thickness has increased to ~14 c/ω_{pe} by 24.25 ω_{LH0}^{-1}, which is equivalent to 0.7 c/ω_{pi} or 0.9 ρ_i. Here c/ω_{pi} and ρ_i are both based on the initial values earthward of the DF. Considering that the earthward density increased slightly by 24.25 ω_{LH0}^{-1}, the actual ion inertial length is smaller than the value at initialization and closer to the DF thickness.

The simulation was run for 24.25ω_{LH}^{-1} or equivalently 1.25Ω_{ci}^{-1}, when the saturated states still hold. In another run that is not shown here, the initial shear scale length is doubled ($L_E = 3.0c/\omega_{pe}$). The electron flow channel width is broadened to 1.9ρ_i or equivalently 1.5c/ω_{pi}. Although the shear frequency is lower than that in the simulation presented here, the EIH instability still develops very well. We present the results for $L_E = 1.5c/\omega_{pe}$ because the physics is similar while the computation is simpler considering that the system length needs to be commensurate with the shear scale length. It is also noteworthy that the flow channel in the saturated stage is shifted in the direction transverse to the flow, which is caused by the force balance. As the electron flow is depleted, the magnetic gradient force compresses the DF, which results in the earthward displacement of the initial DF.

Uniform electron and ion temperatures are used in this simulation study although the temperatures typically have a gradient across the DF in satellite observations and self-consistently formed DFs (e.g., Lu, Artemyev, et al., 2016; Runov et al., 2009, 2011). However, the temperature gradient in the MMS observation of DF reported by Ganguli et al. (2018) is negligible. This event is used in our simulation because its equilibrium physics is thoroughly analyzed thus provides a firm basis to study the nonlinear evolution. On the other hand, the temperature gradient in DF is usually found to be in the opposite direction to the density gradient, which reduces the pressure gradient and hence the diamagnetic drift but not the ambipolar electric field driven $\vec{E} \times \vec{B}$ drift. This will further enhance the EIH waves and retard the LH drift or other pressure gradient-driven waves.

The higher plasma β in the study of EIH dependence on β is achieved by increasing the temperature of electrons and ions while keeping the other parameters such as the shear scale length L_E the same. The challenge of using a larger β in the simulation is that the shear scale length and the system length have to increase accordingly with the electron/ion gyro radius while the electron gyroradius has to be resolved to achieve the $\vec{E} \times \vec{B}$ drift motion. Considering that DF thickness is usually comparable to the ion gyroradius, a larger plasma β may imply a thicker DF boundary layer thus a lower shear frequency. Here we control the variables such as L_E to highlight that with increasing β, the wavelengths of the EIH waves become longer, and they become increasingly electromagnetic. This is important since although the power in DF emission is mostly in the electrostatic regime, there is also some power in the electromagnetic regime. The velocity shear-generated EIH waves display this character. This has important physics implications since it implies that most of the energy goes into particle energization in the DF frame as the electrostatic power dissipates rather than be transported away from the DF as Poynting flux by the electromagnetic waves.

When the DFs are propagating toward the Earth, there is a convection electric field along the dusk direction. In this study, the EIH instability is investigated in the reference frame moving with the DF; thus, there is

no convection electric field in the dawn-dusk direction. The ambipolar electric field along the X direction is not affected by the earthward motion.

The DF configuration adopted in this simulation is simplified; however, it retains the critical aspects of the DF. A three-dimensional PIC model starting from magnetotail current sheet configuration may provide a global view of the DF that is self-consistently generated from the magnetotail reconnection with earthward propagation effects. However, the EIH mechanism discussed in this study is essentially on the kinetic scale and a locally dissipative process. It requires resolving the electron-ion charge separation scale and time scale much below the ion gyroperiod. A local EMPIC model is sufficient for such a purpose. Achieving such resolution in a global PIC model is still not practical.

This study provides the first electromagnetic kinetic simulation of the local dissipation in DF due to velocity inhomogeneities. It is highlighted that the velocity shear substantially contributes to the wave emissions at the magnetotail DFs. The EIH mechanism is suggested to be responsible for the generation of broadband LH waves at DFs. The transition of the EIH instability to more electromagnetic fluctuations with increasing plasma β implies that the waves with more electromagnetic properties could propagate away from the DF and may affect other magnetospheric particle populations. The shear-driven wave modes have implications for the energy dissipation and particle dynamics at the DF. Recent theoretical advances show that the EIH-driven waves are formally electromagnetic especially when the wave vector has a finite parallel component (Ganguli et al., 2014). In order to fully characterize the electrostatic and electromagnetic effects of the shear-driven emissions at the DF, it is necessary to extend the current 2-D model to 3-D and global model and consider a broader range of plasma parameters in the future. Whistler mode waves are also suggested to be excited by the velocity shear when there is a finite parallel component of wave vector (Ganguli et al., 2014). Since the magnetic field enhancement at DFs is often preceded by a decrease (e.g., Liu et al., 2013; Lu, Artemyev, et al., 2016; Shi et al., 2014), it is also necessary to consider how the DF dip could affect the particle distribution and velocity shear at the DF.

Acknowledgments
This study was funded by NASAMAG16_2-0050. The authors acknowledge Advanced Research Computing (ARC) at Virginia Tech and the Space Computer Center (SpaceCC) of the Electrical and Computer Engineering Department for providing computational resources and technical support that have contributed to the results reported within this paper. The model outputs that are used in this paper are being preserved in a Virginia Tech data repository and can be accessed publicly at their website (https://computing.ece.vt.edu/~ldong7/).

References

Amatucci, W. E., Walker, D., Ganguli, G., Antoniades, J., Duncan, D., Bowles, J., et al. (1996). Plasma response to strongly sheared flow. *Physical Review Letters*, *77*(10), 1978–1981. https://doi.org/10.1103/PhysRevLett.77.1978

Daughton, W. (2003). Electromagnetic properties of the lower-hybrid drift instability in a thin current sheet. *Physics of Plasmas*, *10*(8), 3103–3119. https://doi.org/10.1063/1.1594724

Divin, A., Khotyaintsev, Y. V., Vaivads, A., & André, M. (2015). Lower hybrid drift instability at a dipolarization front. *Journal of Geophysical Research: Space Physics*, *120*, 1124–1132. https://doi.org/10.1002/2014JA020528

Divin, A., Khotyaintsev, Y. V., Vaivads, A., André, M., Markidis, S., & Lapenta, G. (2015). Evolution of the lower hybrid drift instability at reconnection jet front. *Journal of Geophysical Research: Space Physics*, *120*, 2675–2690. https://doi.org/10.1002/2014JA020503

DuBois, A. M., Thomas, E., Amatucci, W. E., & Ganguli, G. (2014). Experimental characterization of broadband electrostatic noise due to plasma compression. *Journal of Geophysical Research: Space Physics*, *119*, 5624–5637. https://doi.org/10.1002/2014JA020198

Fletcher, A. C., Crabtree, C., Ganguli, G., Malaspina, D., Tejero, E., & Chu, X. (2019). Kinetic equilibrium and stability analysis of dipolarization fronts. *Journal of Geophysical Research: Space Physics*, *124*, 2010–2028. https://doi.org/10.1029/2018JA026433

Fu, H. S., Khotyaintsev, Y. V., André, M., & Vaivads, A. (2011). Fermi and betatron acceleration of suprathermal electrons behind dipolarization fronts. *Geophysical Research Letters*, *38*, L16104. https://doi.org/10.1029/2011GL048528

Fu, H. S., Khotyaintsev, Y. V., Vaivads, A., André, M., & Huang, S. (2012). Electric structure of dipolarization front at sub-proton scale. *Geophysical Research Letters*, *39*, L06105. https://doi.org/10.1029/2012GL051274

Fu, H. S, Khotyaintsev, Y., Vaivads, A., André, M., Sergeev, V., Huang, S., et al. (2012). Pitch angle distribution of suprathermal electrons behind dipolarization fronts: A statistical overview. *Journal of Geophysical Research*, *117*, A12221. https://doi.org/10.1029/2012JA018141

Ganguli, G., Crabtree, C., Fletcher, A. C., Tejero, E., Malaspina, D., & Cohen, I. (2018). Kinetic equilibrium of dipolarization fronts. *Scientific Reports-UK*, *8*(1), 17186. https://doi.org/10.1038/s41598-018-35349-9

Ganguli, G., Keskinen, M. J., Romero, H., Heelis, R., Moore, T., & Pollock, C. (1994). Coupling of microprocesses and macroprocesses due to velocity shear: An application to the low-altitude ionosphere. *Journal of Geophysical Research*, *99*(A5), 8873–8889. https://doi.org/10.1029/93JA03181

Ganguli, G., Lee, Y., & Palmadesso, P. (1988a). Kinetic theory for electrostatic waves due to transverse velocity shears. *Physics of Fluids*, *31*(4), 823–838. https://doi.org/10.1063/1.866818

Ganguli, G., Lee, Y., & Palmadesso, P. (1988b). Electron–ion hybrid mode due to transverse velocity shear. *Physics of Fluids*, *31*(10), 2753–2756. https://doi.org/10.1063/1.866982

Ganguli, G., Romero, H., & Fedder, J. (1994). Interaction between global MHD and kinetic processes in the magnetotail. *Washington DC American Geophysical Union Geophysical Monograph Series*, *84*, 135–148. https://doi.org/10.1029/GM084p0135

Ganguli, G., Tejero, E., Crabtree, C., Amatucci, W., & Rudakov, L. (2014). Generation of electromagnetic waves in the very low frequency band by velocity gradient. *Physics of Plasmas*, *21*(1), 012107. https://doi.org/10.1063/1.4862032

Hasegawa, H., Fujimoto, M., Phan, T.-D., Reme, H., Balogh, A., Dunlop, M., et al. (2004). Transport of solar wind into Earth's magnetosphere through rolled-up Kelvin-Helmholtz vortices. *Nature*, *430*(7001), 755.

Huang, C., Wu, M. ., Lu, Q., Wang, R., & Wang, S. (2015). Electron acceleration in the dipolarization front driven by magnetic reconnection. *Journal of Geophysical Research: Space Physics*, *120*, 1759–1765. https://doi.org/10.1002/2014JA020918

Krall, N. A., & Liewer, P. C. (2014). Low-frequency instabilities in magnetic pulses. *Physical Review A*, *4*(5), 2094–2103. https://doi.org/10.1103/PhysRevA.4.2094

Lapenta, G., & Bettarini, L. (2011). Self-consistent seeding of the interchange instability in dipolarization fronts. *Geophysical Research Letters*, *38*, L11102. https://doi.org/10.1029/2011GL047742

Lin, D., Wang, C., Li, W., Tang, B., Guo, X., & Peng, Z. (2014). Properties of Kelvin-Helmholtz waves at the magnetopause under northward interplanetary magnetic field: Statistical study. *Journal of Geophysical Research: Space Physics*, *119*, 7485–7494. https://doi.org/10.1002/2014JA020379

Liu, J., Angelopoulos, V., Runov, A., & Zhou, X.-Z. (2013). On the current sheets surrounding dipolarizing flux bundles in the magnetotail: The case for wedgelets. *Journal of Geophysical Research: Space Physics*, *118*, 2000–2020. https://doi.org/10.1002/jgra.50092

Liu, Y., Cao, J., Xu, L., Zhang, X., Wang, P., Wang, J., et al. (2014). Coherent structure generated in the boundary layer of a laboratory-created ionospheric depletion. *Geophysical Research Letters*, *41*, 1413–1419. https://doi.org/10.1002/2014GL059211

Liu, C. M., Fu, H. S., Vaivads, A., Khotyaintsev, Y. V., Gershman, D. J., Hwang, K.-J., et al. (2018). Electron jet detected by MMS at dipolarization front. *Geophysical Research Letters*, *45*, 556–564. https://doi.org/10.1002/2017GL076509

Liu, Y., Lei, J., Yu, P., Zhang, Z., Zhang, X., & Cao, J. (2017). Laboratory generation of broadband ELF waves by inhomogeneous plasma flow. *Geophysical Research Letters*, *44*, 1634–1640. https://doi.org/10.1002/2016GL072232

Lu, S., Angelopoulos, V., & Fu, H. (2016). Suprathermal particle energization in dipolarization fronts: Particle-in-cell simulations. *Journal of Geophysical Research: Space Physics*, *121*, 9483–9500. https://doi.org/10.1002/2016JA022815

Lu, S., Artemyev, A., Angelopoulos, V., Lu, Q., & Liu, J. (2016). On the current density reduction ahead of dipolarization fronts. *Journal of Geophysical Research: Space Physics*, *121*, 4269–4278. https://doi.org/10.1002/2016JA022754

Lu, S., Lu, Q., Lin, Y., Wang, X., Ge, Y., Wang, R., et al. (2015). Dipolarization fronts as Earthward propagating flux ropes: A three-dimensional global hybrid simulation. *Journal of Geophysical Research: Space Physics*, *120*, 6286–6300. https://doi.org/10.1002/2015JA021213

Pritchett, P., & Coroniti, F. (2010). A kinetic ballooning/interchange instability in the magnetotail. *Journal of Geophysical Research*, *115*, A06301. https://doi.org/10.1029/2009JA014752

Romero, H., & Ganguli, G. (1993). Nonlinear evolution of a strongly sheared cross-field plasma flow. *Physics of Fluids B: Plasma Physics*, *5*(9), 3163–3181. https://doi.org/10.1063/1.860653

Romero, H., Ganguli, G., Lee, Y., & Palmadesso, P. (1992). Electron–ion hybrid instabilities driven by velocity shear in a magnetized plasma. *Physics of Fluids B: Plasma Physics*, *4*(7), 1708–1723. https://doi.org/10.1063/1.860028

Runov, A., Angelopoulos, V., Sitnov, M., Sergeev, V., Bonnell, J., McFadden, J., et al. (2009). THEMIS observations of an Earthward-propagating dipolarization front. *Geophysical Research Letters*, *36*, L14106. https://doi.org/10.1029/2009GL038980

Runov, A., Angelopoulos, V., Zhou, X.-Z., Zhang, X.-J., Li, S., Plaschke, F., & Bonnell, J. (2011). A THEMIS multicase study of dipolarization fronts in the magnetotail plasma sheet. *Journal of Geophysical Research*, *116*, A05216. https://doi.org/10.1029/2010JA016316

Scales, W. A., Bernhardt, P., & Ganguli, G. (1994). Early time evolution of negative ion clouds and electron density depletions produced during electron attachment chemical release experiments. *Journal of Geophysical Research*, *99*(A1), 373–381. https://doi.org/10.1029/93JA02752

Scales, W., Bernhardt, P., Ganguli, G., Siefring, C., & Rodriguez, P. (1994). Small-scale plasma irregularities produced during electron attachment chemical releases. *Geophysical Research Letters*, *21*(7), 605–608. https://doi.org/10.1029/94GL00369

Schmid, D., Volwerk, M., Nakamura, R., Baumjohann, W., & Heyn, M. (2014). A statistical and event study of magnetotail dipolarization fronts. *Annals of Geophysics*, *29*(9), 1537–1547. https://doi.org/10.5194/angeo-29-1537-2011

Shi, X., Chen, T., Zhang, L., Duan, S., Liu, J., & He, Z. (2014). Ion flux dropout observed near dipolarization front. *Chinese Science Bulletin*, *59*(34), 4790–4796. https://doi.org/10.1007/s11434-014-0616-8

Sitnov, M., Swisdak, M., & Divin, A. (2009). Dipolarization fronts as a signature of transient reconnection in the magnetotail. *Journal of Geophysical Research*, *114*, A04202. https://doi.org/10.1029/2008JA013980

Wu, P., & Shay, M. A. (2012). Magnetotail dipolarization front and associated ion reflection: Particle-in-cell simulations. *Geophysical Research Letters*, *39*, L08107. https://doi.org/10.1029/2012GL051486

Zhang, X., Angelopoulos, V., Artemyev, A., & Liu, J. (2018). Whistler and electron firehose instability control of electron distributions in and around dipolarizing flux bundles. *Geophysical Research Letters*, *45*, 9380–9389. https://doi.org/10.1029/2018GL079613

Zhou, M., Ashour-Abdalla, M., Deng, X., Schriver, D., El-Alaoui, M., & Pang, Y. (2009). THEMIS observation of multiple dipolarization fronts and associated wave characteristics in the near-Earth magnetotail. *Geophysical Research Letters*, *36*, L20107. https://doi.org/10.1029/2009GL040663